Emergence and Ordering of Polygonal Breathers in Polariton Condensates

Samuel N. Alperin[1] and Natalia G. Berloff[1,2,*]
[1]Department of Applied Mathematics and Theoretical Physics, University of Cambridge, Cambridge CB3 0WA, United Kingdom
[2]Skolkovo Institute of Science and Technology Novaya Street, 100, Skolkovo 143025, Russian Federation

(Received 10 May 2021; accepted 24 May 2022; published 27 June 2022)

We show that the simultaneous driving of a polariton condensate with both nonresonant and nth order resonant pump frequencies allows for a generic mechanism of breather formation. From this we construct for the second order resonance a family of exotic breathers with nontrivial discrete order of rotational symmetry. Finally, we demonstrate the spontaneous emergence of both crystalline and glassy orderings of lattices of polygonal breathers, depending on the degree of polygonal excitations at the lattice sites.

DOI: 10.1103/PhysRevLett.129.015301

Introduction.—The basic nonlinear excitations of Bose-Einstein condensates (BECs) have been studied in detail for decades [1–10]. However, relatively little is understood about their breather solutions [11]. In atomic BECs, there are fundamental restrictions on the formation and stability of breathers, due to their intrinsic tendency toward thermodynamic equilibrium. Solutions with sustained density oscillations can be constructed by the superposition of the ground state with one of the eigenstates of the Bogoliubov excitations. However, these simple periodic solutions are only persistent in the limit of zero amplitude so as to avoid damping via nonlinear spectral broadening, and lose periodicity as modes are mixed [11]. Other simple breathing solutions have been constructed with the help of explicit periodicity of the potential in space [12] or of the interaction term in time [13]. In a nonperiodic system, it was shown that in two spatial dimensions the nonlinear Schrödinger equation under harmonic trapping admits solutions in which the potential energy oscillates without damping, due to the SO(2,1) dynamical symmetry of that system [14,15]. This has recently been extended experimentally and theoretically showing that the SO(2,1) symmetric system also allows particular solutions that are periodic in the wave function evolution [11,16].

Because of its inherent nonequilibriation and strong nonlinearity, BEC of exciton-polariton (polariton) quasiparticles has quickly established itself as a central object of study in nonequilibrium quantum dynamics [17–19]. By their nature these condensates are not required to conserve particle number, their populations instead ebbing and flowing as a part of their dynamics. Even in the steady state the constant dissipation and excitation of quasiparticles makes for a quantum fluidic system in which stationary flows connect spatial regions from where particles are created to where they dissipate. To form and sustain a polariton condensate, the cavity in which it lives must be forced optically. Thus, understanding the fundamental repercussions of the forcing type is among the most fundamental problems in the rapidly growing field of polaritonics.

In this Letter, we show that in polariton BECs a generic mechanism of breather formation arises from the combination of nonresonant and resonant forcing, due to the competition between the distinct symmetries associated with these forcing types. Focusing on the special case of second-order resonance (maximizing the tension between forcing symmetries), we both explain the recent discovery of breathing ring solitons [20], and construct a new family of breathers, in which rotational symmetry is spontaneously broken in lieu of polygonal (dihedral) spatial symmetry, with the degree of the resulting polygonal breathers set by the spatial extent of resonant pumping. We show that lattices of the emergent polygonal breathers can spontaneously adopt crystalline or glassy orderings of their orientation, in spinless analogs of ferromagnetic and spin glass orderings.

Generic breathing mechanism.—A prototypical example of the condensed Bose gas driven far from equilibrium, the dynamics of the polariton condensate can be well described by a generalized complex Ginzburg-Landau equation. This can be written nondimensionally for the condensate wave function $\psi(\boldsymbol{r},t)$ and for the reservoir of uncondensed particles $N_R(\boldsymbol{r},t)$, as [18,21–24]:

$$i\partial_t\psi = -(1-i\eta N_R)\nabla^2\psi + |\psi|^2\psi + gN_R\psi + i(N_R-\gamma)\psi + i\bar{P}\psi^{*(n-1)} \tag{1}$$

$$\partial_t N_R = P - (1+b|\psi|^2)N_R, \tag{2}$$

where g characterizes the polariton-exciton interaction strength, η the energy relaxation [25,26], b is proportional to the ratio of polariton-reservoir to polariton-polariton interactions and inversely proportional to the reservoir scattering rate, and where γ represents rate of dissipation. The nonresonant pump source is given by pump intensity $P(\boldsymbol{r},t)$, and the resonant pumping (at n:1 resonance with

the natural frequency of the cavity) is described by the pumping intensity $\bar{P}(\boldsymbol{r}, t)$ [27]. In these dimensionless units, the healing length is unity while the unit of length is 1 μm.

We begin by focusing on the regime in which the reservoir dynamics react quickly to the condensate wave function ($\partial_t N_R \approx 0$), in which the energy relaxation $\eta \ll 1$, and in which $b \approx 1$. From here we insert $N_R = P/(1 + |\psi|^2)$ into Eq. (2); focusing first on the behavior of the system in zero-dimensional space, the dynamics of the polariton condensate are reduced to the following complex ordinary differential equation:

$$i\dot{\psi} = \frac{(1 - i\gamma)|\psi|^2 + |\psi|^4 - i\gamma + (g + i)P}{(|\psi|^2 + 1)/\psi} + i\bar{P}\psi^{*(n-1)}. \quad (3)$$

Introducing the Madelung transformation $\psi(t) = \sqrt{\rho(t)}\exp[i\theta(t)]$ and separating real and imaginary parts of the resulting equation, we can rewrite Eq. (3) as the real, coupled ordinary differential equations

$$\dot{\rho} = 2\frac{\bar{P}\cos(n\theta)(\rho^{\frac{n}{2}} + \rho^{\frac{n}{2}+1}) + (P - \gamma)\rho - \gamma\rho^2}{(1 + \rho)}, \quad (4)$$

$$\dot{\theta} = \frac{\bar{P}\sin(n\theta)(\rho^{\frac{n}{2}-1} - \rho^{\frac{n}{2}}) - gP - \rho - \rho^2}{(1 + \rho)}. \quad (5)$$

Physically, ρ represents the time dependent condensate wave function density and θ its phase. Equations (4) and (5) are not explicitly solvable, but in the limit of small resonant pump strength $\bar{P}$, we can view solutions as perturbations of the steady states familiar to purely nonresonantly pumped condensates. Such nonzero steady states have constant phase evolution $\theta = \mu t$, with frequency μ. Substituting into Eq. (5) and setting $n = 2$ yields the small $\bar{P}$ approximation for the condensate density under simultaneous nonresonant and second-order resonant forcing

$$\rho(t) = \frac{1}{2}\left(\sqrt{\xi(t)^2 - 4[gP + \xi(t)]} - \xi(t) - 1\right) \quad (6)$$

in which $\xi(t) = 1 + \mu + \bar{P}\sin(2\mu t)$. From here, it is clear that for $\bar{P} = 0$, $\xi(t)$ reduces to $\mu + 1$ and Eq. (6) returns the familiar steady state solution, with the density fixed by the parameterization. However, for $\bar{P} > 0$ oscillations take hold, with period given by $T = \pi/\mu$, and with amplitude scaling with $\bar{P}$. Later we will see that even in full 2D simulations of Eqs. (1) and (2), these simple predictions remain robust.

In the other extreme is the scenario of very strong resonant pumping. In this case we expect n fixed points; setting the left-hand sides of Eqs. (4) and (5) to zero yields n solutions for θ and one solution for ρ. These are the nth order phase locking solutions. To probe the full range of behaviors beyond these extreme regimes, we numerically integrate Eqs. (4) and (5). As this case is of the greatest interest, we again fix $n = 2$. Integrating for many initial conditions $\{\rho_i, \theta_i\}$, phase space trajectories are collected for varying resonant pump strength $\bar{P}$ (with other system parameters fixed), shown in Fig. 1 (top). The bottom panel of that figure shows some of the same trajectories (matched in color), but represented in the complex plane as opposed to the phase space. In these spaces geometrical interpretations of the effect of resonant pumping, and the resulting density oscillations, become clear. As expected, for $\bar{P} = 0$ (not shown), there is a single fixed point attractor corresponding to a single point of nonzero phase velocity and nonzero density in the phase space, which corresponds to a circular trajectory in the complex plane; this is merely the plane wave solution. At the other extreme, high resonant forcing (orange) leads to a set of two fixed point attractors (resolved in the complex plane) at states with fixed density and null phase velocity (resolved in phase space).

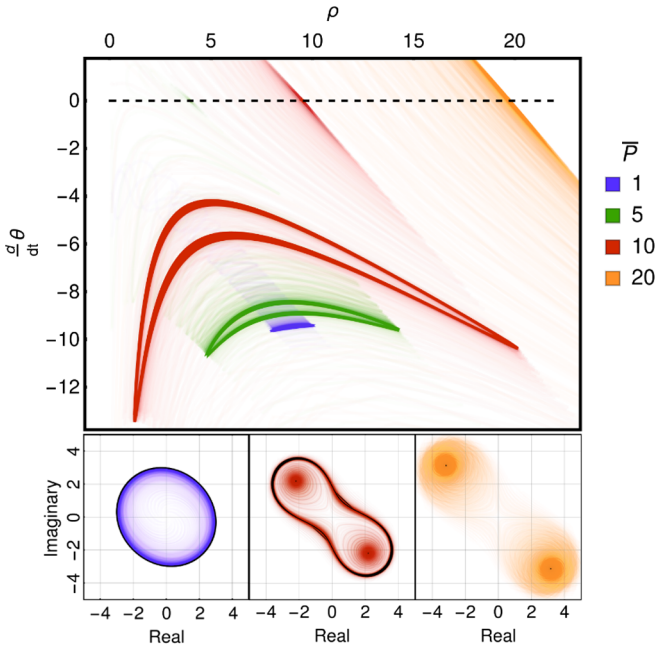

FIG. 1. Top: Trajectories of Eqs. (4) and (5) traced numerically in phase space from many initial conditions, using $\gamma = 1/2$, $P = 5$, and $g = 1$, and various second-order resonant pump strengths $\bar{P} = \{1, 5, 10, 20\}$. The line of zero phase velocity is marked (dashed black). Bottom: The same phase trajectories are plotted in the complex plane showing transition from small, nearly uniform oscillations driven by small resonant pumping (blue), to the dual fixed point attractors seen under high resonant forcing (orange). In between, both fixed points and large nonuniform density oscillations are seen (red).

The most interesting behavior is seen between these extremes. As the resonant forcing strength is increased gradually from zero, the smooth "stretching" of the closed state trajectories in the complex plane is observed, in the directions of the symmetry broken fixed points that then eventually form. In this way, the geometry of the resonant

forcing terms in Eqs. (4) and (5) are clear: in the complex plane the terms $\bar{P}\cos(n\theta)$ and $\bar{P}\sin(n\theta)$ are linear scaling operators, acting along n axes separated by $2\pi/n$. Thus, we should expect an n-fold stretching of the circular orbit as $\bar{P}$ is increased from zero, and for increasing $\bar{P}$ we should expect the density increasingly dependent on the phase with degeneracy n. Figure 1 confirms these behaviors. For small resonant pumping, we see slight n-fold deformation of the orbit in the complex plane (blue), which becomes severely deformed (but with equal symmetry) as the resonant pumping is increased (red). That case also shows the overlap between the limit cycle and phase locked regimes. We note that the same procedure for any nth order resonance yields the same fundamental result, but showing n-fold symmetry in the complex plane. We confirm this in numerical experiments for $n \in \{1, \ldots, 5\}$. The warping of the phase space trajectories has more than a geometric effect: the noncircular closed path in the complex state space is trivially indicative of density oscillations in the wave function. Thus, it can be useful to think of the orbit deformations as "driving" the density oscillations (and which fully characterizes their wave forms). In this way, breathing is a result of the tension between the two natural states of competing symmetries, the U(1) phase symmetry of $\bar{P} = 0$, and the $\mathbb{Z}_n$ symmetry of large $\bar{P}$. In the Supplemental Material [28] we derive the conditions for the frequency locking in our system with $n = 2$ close to the condensation threshold and perform a linear stability analysis of the rest state to quantify the contributions of different types of excitation to the dispersion relation.

2D breathers.—So far we have established that under the simultaneous resonant and nonresonant forcing of a polariton condensate, there generically exists a regime of density oscillations in between the plane wave and phase locked solutions. We now turn to the full, spatially extended (2D) system. In a system phase locked by strong second-order resonant forcing, there are two equally stable phases differing by π, so that stable one-dimensional topological defects naturally form between domains of opposite phase (domain walls or "dark solitons"). For $n > 2$, more phases become stable, quickly approximating the U(1) symmetry. Thus, from the perspective of pattern formation, the second-order resonant forcing is the most extreme case, as the associated $\mathbb{Z}_2$ symmetry is the starkest departure from U(1) while maintaining the necessary degeneracy. Thus, while the our breathing mechanism applies to higher resonances, in the 2D case we will focus only the second-order resonant forcing.

We begin this by considering the condensate forced uniformly with nonresonant and second-order resonant (from this point "resonant") forcing. It was recently shown that ring-shaped breathers can form in such a system [20], and we now show that these result from the breathing mechanism described in this Letter. In full numerical integration of Eqs. (1) and (2) [27], we prepare a uniform disk-shaped condensate pumped with resonant forcing high enough to reach the regime of phase locking. By phase imprinting a perturbation, we observe the excitations of a breathing ring soliton, as shown in Fig. 2, which have the periodicity π/μ as predicted in the zero-dimensional problem. These structures may thus be interpreted as the localized excitations of the phase locked state into the limit cycle in a phase space which, as in the zero-dimensional space, admits both simultaneously.

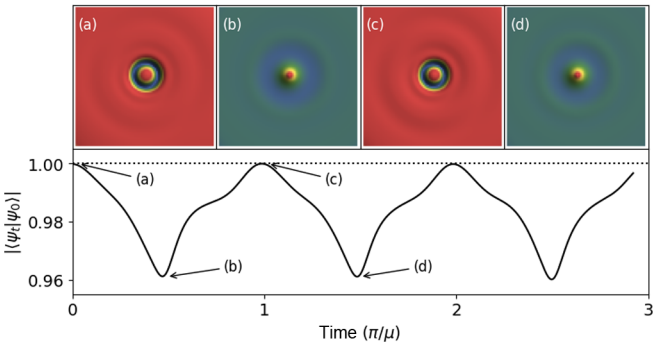

FIG. 2. Panels (a)–(d): Density of breathing ring soliton at several times, excited by a phase imprinted perturbation in the uniform condensate, forced homogenously with nonresonant and second-order resonant pumping. Bottom: Overlap between the evolving wave function of the condensate and that at the time fixed at (a), showing the periodicity of the complex wave function. $P = \bar{P} = 5$.

Polygon breathers.—One of the powers of polaritonic systems is that pumping can take on any optically feasible profile. We can thus consider the case of spatially dependent resonant forcing, so that the degree to which the phase is symmetry broken can vary spatially.

We thus consider the scenario of a large disk-shaped region of uniform nonresonant pumping, with a resonant pump of Gaussian profile $\bar{P}\exp[-\alpha r^2]$ at the center of that region, with α characterizing the inverse width of the pump, so that the degree of the symmetry breaking of the phase depends on the radial distance from the center of the pump. This is the most extreme when $\bar{P}$ and α are chosen such that the condensate wave function is forced into the phase locked regime at the center, but can be seen to transition into the regime in which the symmetry breaking is negligible. With direct numerical integration of Eqs. (1) and (2), we simulate this geometry. For large α (small spot), density oscillations are driven around the center at the radius at which the condensate is in the breathing regime, forming a breathing ring.

For larger resonant pump spots, however, the behavior changes drastically: as the pump spot width is increased (keeping $\bar{P}$ constant), the radius of the dark ring increases, and existing out of the bistable regime, reaches the circumference at which the ring becomes unstable to the "snake instability," the well-known phenomenon in which azimuthal modes of the annular defect shatter the dark soliton into

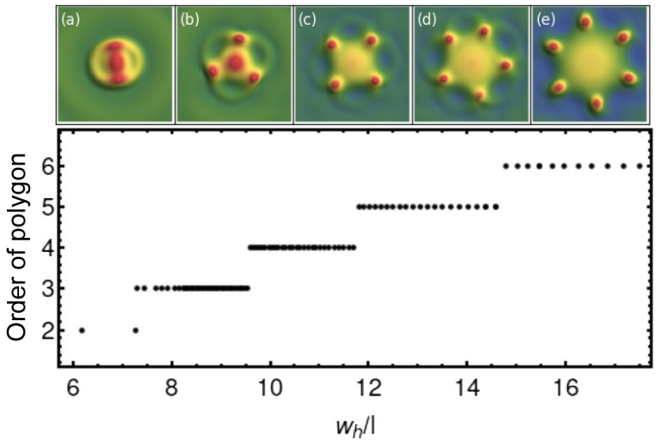

FIG. 3. Panels (a)–(e): From direct numerical integration of Eqs. (1) and (2), density profiles exhibiting $m \in \{2, \ldots, 6\}$ spatial symmetry, adopted spontaneously for fixed homogenous nonresonant pump ($P = 2$) and second-order resonant pumping with Gaussian profile $\bar{P}\exp[-\alpha r^2]$ at fixed strength ($\bar{P} = 15$) and varying half-width parameter α. Bottom: Corresponding dependence of spontaneously adopted symmetry order m on the Gaussian half-width in units of the healing length.

an integer number of chiral defects [34,35]. This instability thus naturally quantizes the number of vortex-antivortex pairs produced as a function of the ring radius. This quantization is demonstrated in Fig. 3, which shows the dependence of the emergent polygonal symmetry as a function of the Gaussian half width at half maximum (half-width) in units of healing lengths, as determined from numerical experiments. The half-width is defined as $w_h = \sqrt{\log(2)/\alpha}$.

Once the rotational symmetry breaks after a finite number of oscillation cycles, the symmetry remains broken, and a new dynamically stable structure is formed which, though evolving dynamically, is at every time symmetric under transformations of the dihedral group D_m (the group of symmetry transformations of the polygon of degree m). Figure 4 shows density profiles of two polygonal breathers at several times during their evolutions. The bottom panel of that figure shows the inner product $|\langle\psi_0|\psi_t\rangle| = (1/A)|\int \psi^*(\boldsymbol{r}, 0)\psi(\boldsymbol{r}, t)d\boldsymbol{r}|$ (where A is chosen such that $|\langle\psi_0|\psi_0\rangle| = 1$) of the $m = 4$ (square-symmetric) breather, where we arbitrarily set ψ_0 to the wave function at the time shown in (a). The wave function indeed forms a closed periodic cycle once the symmetry has broken, despite the rotational symmetry of the physical system. The periodicity of the breather is almost exactly equal to twice the predicted periodicity of the density oscillations studied in 0D. This period doubling comes from the broken rotational symmetry of the structure: $|\psi(t)\rangle = R(\pi/m)|\psi(t + \pi/\mu)\rangle$, where the operator $R(\phi)$ rotates the breather by ϕ radians about its center, so that $|\psi(t)\rangle = |\psi(t + 2\pi/\mu)\rangle$.

Orientation glass.—While these spontaneously polygon-symmetric excitations are translationally fixed by the

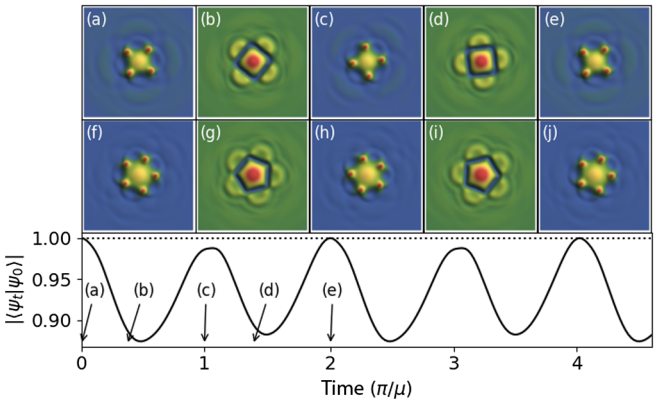

FIG. 4. From direct numerical integration of Eqs. (1) and (2), density profiles over the evolution of two breathing structures exhibiting different degrees of quantized spatial symmetry breaking, under uniform nonresonant pumping $P = 2$ and a Gaussian $n = 2$ resonant pump of the form $\bar{P}\exp[-\alpha r^2]$, with $\bar{P} = 10$. (a)–(e) show the dynamics of the breather formed when $\alpha = 0.05$, which spontaneously adopts degree-4 polygonal symmetry, and then evolves in a closed cycle: the bottom panel shows the inner product of the condensate wave function over time with that shown in (a), showing that the wave function perfectly repeats periodically. (f),(j) show the evolution of a degree-5 symmetric breather, formed spontaneously when $\alpha = 0.03$.

location of a Gaussian resonant pump, they do posses a rotational degree of freedom. The polygonal structures radiate density oscillations possessing the polygonal symmetry of their source indicating the emergence of orientational order in a lattice of polygonal breathers. Figure 5 shows the direct numerical simulation of a condensate forced by uniform nonresonant pumping and by a square lattice of Gaussian pumps with inverse width parameter α.

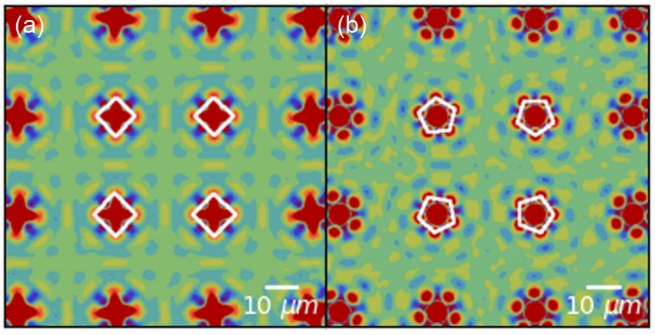

FIG. 5. Condensate densities under uniform nonresonant pumping, simultaneously pumped by a square lattice of resonant pumps with Gaussian profile $\bar{P}\exp[-\alpha r^2]$. Orientations of central lattice site excitations highlighted in white. (a) Spontaneous orientational order emerges when α is chosen such that the lattice site excitations match the symmetry of the lattice. (b) A glassy ordering emerges instead when α is chosen such that the symmetry of the lattice site excitations is incommensurate with that of the lattice. $P = 1.5$ and $\bar{P} = 10$. $\alpha = 0.1$ in (a) and $\alpha = 0.075$ in (b).

When α is chosen such that the lattice sites exhibit square-symmetric excitations, the symmetries of the excitations and the lattice are commensurate and spontaneously align (a). When α is instead chosen such that the lattice sites exhibit pentagonal symmetry, the symmetries of the lattice and the lattice sites are incommensurate, causing geometric frustration resulting in a glassy state. These are the analogs of the ferromagnetic and spin glass states, but where the spin degree of freedom (parameterized by $\mathbb{Z}_n$ for discrete spins) is replaced by the polygonal orientation degree of freedom (parametrized by D_m).

In conclusion, we have introduced a generic mechanism of breather formation in nonequilibrium condensates that leads to highly nontrivial dynamical behavior, including the spontaneous adoption of unusual spatial symmetries and emergent order.

N. G. B. acknowledges the financial support from the John Schwinger Foundation Grant No. JSF-19-02-0005.

*N.G.Berloff@damtp.cam.ac.uk

[1] V. M. Perez-Garcia, H. Michinel, J. I. Cirac, M. Lewenstein, and P. Zoller, Phys. Rev. A **56**, 1424 (1997).
[2] M. R. Matthews, B. P. Anderson, P. C. Haljan, D. S. Hall, C. E. Wieman, and E. A. Cornell, Phys. Rev. Lett. **83**, 2498 (1999).
[3] K. W. Madison, F. Chevy, W. Wohlleben, and J. Dalibard, Phys. Rev. Lett. **84**, 806 (2000).
[4] J. Denschlag, J. E. Simsarian, D. L. Feder, C. W. Clark, L. A. Collins, J. Cubizolles, L. Deng, E. W. Hagley, K. Helmerson, W. P. Reinhardt *et al.*, Science **287**, 97 (2000).
[5] B. P. Anderson, P. C. Haljan, C. A. Regal, D. L. Feder, L. A. Collins, C. W. Clark, and E. A. Cornell, Phys. Rev. Lett. **86**, 2926 (2001).
[6] Z. Dutton, M. Budde, C. Slowe, and L. V. Hau, Science **293**, 663 (2001).
[7] A. A. Penckwitt, R. J. Ballagh, and C. W. Gardiner, Phys. Rev. Lett. **89**, 260402 (2002).
[8] O. Morsch and M. Oberthaler, Rev. Mod. Phys. **78**, 179 (2006).
[9] E. A. L. Henn, J. A. Seman, G. Roati, K. M. F. Magalhaes, and V. S. Bagnato, Phys. Rev. Lett. **103**, 045301 (2009).
[10] N. Navon, A. L. Gaunt, R. P. Smith, and Z. Hadzibabic, Nature (London) **539**, 72 (2016).
[11] R. Saint-Jalm, P. C. M. Castilho, É. Le Cerf, B. Bakkali-Hassani, J.-L. Ville, S. Nascimbene, J. Beugnon, and J. Dalibard, Phys. Rev. X **9**, 021035 (2019).
[12] A. Trombettoni and A. Smerzi, Phys. Rev. Lett. **86**, 2353 (2001).
[13] M. Matuszewski, E. Infeld, B. A. Malomed, and M. Trippenbach, Phys. Rev. Lett. **95**, 050403 (2005).
[14] L. P. Pitaevskii and A. Rosch, Phys. Rev. A **55**, R853 (1997).
[15] F. Chevy, V. Bretin, P. Rosenbusch, K. W. Madison, and J. Dalibard, Phys. Rev. Lett. **88**, 250402 (2002).
[16] C. Lv, R. Zhang, and Q. Zhou, Phys. Rev. Lett. **125**, 253002 (2020).
[17] H. Deng, H. Haug, and Y. Yamamoto, Rev. Mod. Phys. **82**, 1489 (2010).
[18] J. Keeling and N. G. Berloff, Contemp. Phys. **52**, 131 (2011).
[19] T. Byrnes, N. Y. Kim, and Y. Yamamoto, Nat. Phys. **10**, 803 (2014).
[20] S. N. Alperin and N. G. Berloff, Phys. Rev. A **102**, 031304 (R) (2020).
[21] K. P. Kalinin and N. G. Berloff, Phys. Rev. Lett. **121**, 235302 (2018).
[22] J. Keeling and N. G. Berloff, Phys. Rev. Lett. **100**, 250401 (2008).
[23] M. Wouters and I. Carusotto, Phys. Rev. Lett. **99**, 140402 (2007).
[24] I. Carusotto and C. Ciuti, Rev. Mod. Phys. **85**, 299 (2013).
[25] M. Wouters, New J. Phys. **14**, 075020 (2012).
[26] N. Berloff and J. Keeling, in *Physics of Quantum Fluids* (Springer, New York, 2013), pp. 19–38.
[27] We use fourth-order Runge-Kutta integration, with the physical parameters $\eta = 0.3$, $g = 1$, and with $\gamma = 0.3$.
[28] See Supplemental Material at http://link.aps.org/supplemental/10.1103/PhysRevLett.129.015301 for a derivation of frequency locking conditions for $n = 2$ and for stability analyses, which includes Refs. [29–33].
[29] P. Coullet and K. Emilsson, Physica (Amsterdam) **61D**, 119 (1992).
[30] A. Yochelis, C. Elphick, A. Hagberg, and E. Meron, Physica (Amsterdam) **199D**, 201 (2004).
[31] L. M. Pismen, *Patterns and Interfaces in Dissipative Dynamics* (Springer-Verlag, Berlin, Heidelberg, 2006).
[32] S. S. Gavrilov, A. S. Brichkin, S. I. Novikov, S. Höfling, C. Schneider, M. Kamp, A. Forchel, and V. D. Kulakovskii, Phys. Rev. B **90**, 235309 (2014).
[33] M. Wouters, Phys. Rev. B **77**, 121302(R) (2008).
[34] G. Theocharis, D. J. Frantzeskakis, P. G. Kevrekidis, B. A. Malomed, and Y. S. Kivshar, Phys. Rev. Lett. **90**, 120403 (2003).
[35] L. D. Carr and C. W. Clark, Phys. Rev. A **74**, 043613 (2006).